Available online at www.sciencedirect.com
ScienceDirect
Journal of Computational Physics 224 (2007) 208–221
JOURNAL OF COMPUTATIONAL PHYSICS
www.elsevier.com/locate/jcp

On a robust discontinuous Galerkin technique for the solution of compressible flow

M. Feistauer *, V. Kučera

Charles University Prague, Faculty of Mathematics and Physics, Sokolovská 83, 186 75 Praha, Czech Republic

Received 11 September 2006; received in revised form 22 January 2007; accepted 25 January 2007
Available online 9 February 2007

Dedicated to Professor Pieter Wesseling on the occasion of his 65th birthday.

Abstract

In the paper, we describe a numerical technique allowing the solution of compressible inviscid flow with a wide range of Mach numbers. The method is based on the application of the discontinuous Galerkin finite element method for the space discretization of the Euler equations written in the conservative form, combined with a semi-implicit time discretization. Special attention is paid to the treatment of boundary conditions and to the stabilization of the method in the vicinity of discontinuities avoiding the Gibbs phenomenon. As a result we obtain a technique allowing the numerical solution of flows with practically all Mach numbers without any modification of the Euler equations. This means that the proposed method can be used for the solution of high speed flows as well as low Mach number flows. Presented numerical tests prove the accuracy of the method and its robustness with respect to the Mach number.

PACS: 02.60.Cb; 02.70.Dh

MSC: 65M60; 76N10

Keywords: Compressible Euler equations; Discontinuous Galerkin space discretization; Vijayasundaram numerical flux; Semi-implicit linearized numerical scheme; Stabilization of the scheme; Low Mach number flow; High speed flow

1. Introduction

In the numerical solution of compressible flow, it is necessary to overcome several obstacles. Let us mention the necessity to resolve accurately shock waves, contact discontinuities and (in viscous flow) boundary layers, wakes and their interaction. All these phenomena are connected with the simulation of high speed flow with

* Corresponding author. Tel.: +420 2 2191 3388; fax: +420 2 2481 1036.
E-mail addresses: feist@karlin.mff.cuni.cz (M. Feistauer), vaclav.kucera@email.cz (V. Kučera).

0021-9991/$ - see front matter
doi:10.1016/j.jcp.2007.01.035

high Mach numbers. However, it appears that the solution of low Mach number flow is also rather difficult. This is caused by the stiff behaviour of numerical schemes and acoustic phenomena appearing in low Mach number flows at incompressible limit. In this case, standard finite volume schemes fail. This led to the development of special finite volume techniques allowing the simulation of compressible flow at incompressible limit, which are based on modifications of the Euler or Navier–Stokes equations. We can mention works by Klein, Munz, Meister, Wesseling and their collaborators (see, e.g. [17,21], [19] Chapter 5, or [26], Chapter 14). However, these techniques could not be applied to the solution of high speed flow. Therefore, further attempts were concentrated on the extension of these methods to the solution of flows at all speeds. A success in this direction was achieved by several authors. Let us mention, for example, the works by Wesseling et al. [22,25,27], Parker and Munz [20], Meister [18] and Darwish et al. [4]. Main ingredients of these techniques are finite volume schemes applied on staggered grids, combined with multigrid, the use of the pressure-correction, multiple pressure variables and flux preconditioning.

In our paper, we describe a new numerical technique allowing the solution of compressible flow with a wide range of the Mach number without any modification of the governing equations, written in the conservation form with conservative variables. This technique is based on the *discontinuous Galerkin finite element method* (DGFEM), which can be considered as a generalization of the finite volume as well as finite element methods, using advantages of both these techniques. It employs piecewise polynomial approximations without any requirement on the continuity on interfaces between neighbouring elements.

The DGFEM was used for the numerical simulation of the compressible Euler equations by Bassi and Rebay in [1], where the space DG discretization was combined with explicit Runge–Kutta time discretization. In [2] Baumann and Oden describe an *hp* version of the space DG discretization with explicit time stepping to compressible flow. Van der Vegt and van der Ven apply space–time discontinuous Galerkin method to the solution of the Euler equations in [23], where the discrete problem is solved with the aid of a multigrid accelerated pseudo-time-integration. For a survey of DGFE techniques we refer the reader to [3].

In most of works, explicit Euler or Runge–Kutta time discretization is used. Explicit time stepping for the solution of the Euler equations is very popular particularly in the framework of the finite difference and finite volume schemes. Its advantage is a simple algorithmization. However, it requires to satisfy rather restrictive CFL-stability conditions, which is quite inconvenient over nonuniform unstructured anisotropic meshes. Moreover, an explicit time stepping fails in the numerical solution of flows with low Mach numbers at incompressible limit. Therefore, it is suitable to consider implicit methods for the numerical solution of the Euler equations.

In [8] the discontinuous Galerkin space semidiscretization is combined with a semi-implicit time discretization. In this way we obtain an efficient numerical scheme requiring the solution of only one linear system on each time level. It was shown in [8] that the proposed technique is applicable to the solution of stationary as well as nonstationary flow, the accuracy was established and the efficiency was proven in comparison with explicit Runge–Kutta methods.

Here we extend this approach so that the developed technique allows the solution of compressible flow with a wide range of Mach numbers. We explain important details of the method: the derivation of the scheme based on the DGFE space semidiscretization, higher order semi-implicit time discretization, the treatment of boundary conditions and the limiting of order of accuracy near discontinuities in order to avoid the Gibbs phenomenon. Further, with the aid of test problems we show that the method allows the solution of compressible inviscid flow with a wide range of Mach numbers.

In Section 2 the continuous problem describing inviscid compressible flow is formulated. In Section 3 the discontinuous Galerkin space semidiscretization and semi-implicit time stepping are introduced. Section 4 is concerned with the treatment of boundary conditions. In Section 5, the attention is paid to the stabilization of the scheme in the vicinity of discontinuities. Finally, in Section 6 we present examples of the DGFE solutions of an inviscid compressible flow showing the accuracy and robustness of the method. The summary of results and outlook are contained in Section 7.

The computational results show that the presented method is unconditionally stable and is applicable to the numerical solution of inviscid compressible high speed flow as well as flow with a very low Mach number.

2. Governing equations

Because of simplicity, we shall be concerned with the treatment of two-dimensional flow, but the method can be applied to 3D flow as well. The system of the Euler equations describing 2D inviscid flow can be written in the form

$$\frac{\partial \boldsymbol{w}}{\partial} + \sum_{r=1}^{2} \frac{\partial \boldsymbol{f}_r(\boldsymbol{w})}{\partial_{\ r}} = 0 \quad \text{in} \qquad = \Omega \times (0, \quad), \tag{1}$$

where $\Omega \subset \mathbb{R}^2$ is a bounded domain occupied by gas, $T > 0$ is the length of a time interval,

$$\boldsymbol{w} = (_{v\,1}, \ldots, _{v\,4})^{\mathrm{T}} = (\rho, \rho._{\ 1}, \rho._{\ 2}, \quad)^{\mathrm{T}} \tag{2}$$

is the so-called state vector and

$$\boldsymbol{f}_r(\boldsymbol{w}) = (\rho._{\ r}, \rho._{\ r\ 1} + \delta_{r1}\ \ , \rho._{\ r\ 2} + \delta_{r2}\ \ , (\quad + \quad).{}_{r})^{\mathrm{T}} \tag{3}$$

are the inviscid (Euler) fluxes of the quantity $\boldsymbol{w}$ in the directions $_r$, $r = 1, 2$. We use the following notation: ρ is the density, p is the pressure, E is the total energy, $\boldsymbol{v} = (._1, ._2)$ is the velocity, and δ_r is the Kronecker symbol. The equation of state implies that

$$= (\gamma - 1)(\quad - \rho|\boldsymbol{v}|^2/2). \tag{4}$$

Here $\gamma > 1$ is the Poisson adiabatic constant. The system (1)–(4) is *diagonally hyperbolic*. It is equipped with the initial condition

$$\boldsymbol{w}(\boldsymbol{x}, 0) = \boldsymbol{w}^0(\ ), \qquad \in \Omega, \tag{5}$$

and the boundary conditions, which are treated in Section 4.

We define the flux of the quantity $\boldsymbol{w}$ in the direction $\boldsymbol{n} = (_{\kappa 1}, _{\kappa 2}) \in \ \mathbb{R}^2, _{\kappa 1}^2 + _{\kappa 2}^2 = 1$, by

$$\boldsymbol{F}(\boldsymbol{w}, \boldsymbol{n}) = \sum_{r=1}^{2} \boldsymbol{f}_r(\boldsymbol{w})_{\kappa r} \tag{6}$$

and its Jacobi matrix

$$\boldsymbol{P}(\boldsymbol{w}, \boldsymbol{n}) = \frac{D\boldsymbol{F}(\boldsymbol{w}, \boldsymbol{n})}{D\boldsymbol{w}} = \sum_{r=1}^{2} \boldsymbol{A}_r(\boldsymbol{w})_{\kappa r}, \tag{7}$$

where

$$\boldsymbol{A}_r(\boldsymbol{w}) = \frac{D\boldsymbol{f}_r(\boldsymbol{w})}{D\boldsymbol{w}}, \quad r = 1, 2, \tag{8}$$

are the Jacobi matrices of the mappings $\boldsymbol{f}_s$. It is possible to show that $\boldsymbol{f}_r$, $r = 1, 2$, are homogeneous mappings of order one, which implies that

$$\boldsymbol{f}_r(\boldsymbol{w}) = \boldsymbol{A}_r(\boldsymbol{w})\boldsymbol{w}, \quad r = 1, 2, \tag{9}$$

and

$$\boldsymbol{F}(\boldsymbol{w}, \boldsymbol{n}) = \boldsymbol{P}(\boldsymbol{w}, \boldsymbol{n})\boldsymbol{w}. \tag{10}$$

3. Discretization

3.1. Discontinuous Galerkin space semidiscretization

Let Ω_h be a polygonal approximation of Ω. By T_h we denote a partition of Ω_h consisting of elements $\in \ _i, \ \in$, e.g. triangles or quadrilaterals. ($\subset \ ^+ = \{0, 1, 2, \ldots\}$ is a suitable index set.) By Γ_{ij} we denote a common edge between two neighbouring elements K_i and K_j. We set $r(\ ) = \{i \in \ ; \ _i$ is a neighbour of $\}$.

The boundary $\partial\Omega_t$ is formed by a finite number of faces of elements K_i adjacent to $\partial\Omega_t$. We denote all these boundary faces by S_j, where $i \in \subset \bar{} = \{-1,-2,\ldots\}$. Now we set $\gamma(\ ) = \{i \in ; \text{ is a face of } \in \}$ and $\Gamma_i =$ for $\in$ such that $\subset \partial\ , i \in$. For K_i not containing any boundary face S_j we set $\gamma(\ ) = \emptyset$. Obviously, $r(\ ) \cap \gamma(\ ) = \emptyset$ for all $\in$. Now, if we write $(\ ) = r(\ ) \cup \gamma(\ )$, we have

$$\partial\ = \bigcup_{i \in (\ )} \Gamma_i\,, \quad \partial\ \cap \partial\Omega_t = \bigcup_{i \in \gamma(\ )} \Gamma_i\,. \tag{11}$$

The symbol $\boldsymbol{n}_i = ((\nu i)_1, (\nu i)_2)$ will denote the unit outer normal to ∂K_i on the side Γ_{ij}.

The approximate solution will be sought at each time instant t as an element of the finite-dimensional space

$$\boldsymbol{S}_t = \boldsymbol{S}^{,-1}(\Omega_t, \ _t) = \{.\,;.\mid \in \mathcal{M}(\ ) \quad \forall \in \ _t\}^4, \tag{12}$$

where $\geqslant 0$ is an integer and $P^r(K)$ denotes the space of all polynomials on K of degree $\leqslant r$. Functions $\boldsymbol{\varphi} \in \boldsymbol{S}_t$ are in general discontinuous on interfaces Γ_{ij}. By $\boldsymbol{\varphi}|_{\Gamma_i}$ and $\boldsymbol{\varphi}|_{\Gamma_i}$ we denote the values of $\boldsymbol{\varphi}$ on Γ_{ij} considered from the interior and the exterior of K_i, respectively. The symbols

$$\langle\boldsymbol{\varphi}\rangle_i = \frac{1}{2}(\boldsymbol{\varphi}|_{\Gamma_i} + \boldsymbol{\varphi}|_{\Gamma_i}), \quad [\boldsymbol{\varphi}]_i = \boldsymbol{\varphi}|_{\Gamma_i} - \boldsymbol{\varphi}|_{\Gamma_i} \tag{13}$$

denote the average and jump of a function $\boldsymbol{\varphi}$ on $\Gamma_i = \Gamma_i$.

In order to derive the discrete problem, we multiply (1) by a test function $\boldsymbol{\varphi} \in \boldsymbol{S}_t$, integrate over any element , $\in$, apply Green's theorem and sum over all $\in$. Then we approximate fluxes through the faces Γ_{ij} with the aid of a numerical flux $\boldsymbol{H} = \boldsymbol{H}(\boldsymbol{u}, \boldsymbol{w}, \boldsymbol{n})$ in the form

$$\int_{\Gamma_i} \sum_{r=1}^{2} \boldsymbol{f}_r(\boldsymbol{w}(\ ))(\nu i)_r \cdot \boldsymbol{\varphi}\, \mathrm{d} \approx \int_{\Gamma_i} \boldsymbol{H}(\boldsymbol{w}_t(\ )|_{\Gamma_i}, \boldsymbol{w}_t(\ )|_{\Gamma_i}, \boldsymbol{n}_i) \cdot \boldsymbol{\varphi}\, \mathrm{d}. \tag{14}$$

If we introduce the forms

$$(\boldsymbol{w}_t, \boldsymbol{\varphi}_t)_t = \int_{\Omega_t} \boldsymbol{w}_t \cdot \boldsymbol{\varphi}_t \,\mathrm{d}\boldsymbol{x}, \tag{15}$$

$$\tilde{}_t(\boldsymbol{w}_t, \boldsymbol{\varphi}_t) = -\sum_{\in\ _t} \int \sum_{r=1}^{2} \boldsymbol{f}_r(\boldsymbol{w}_t) \cdot \frac{\partial \boldsymbol{\varphi}_t}{\partial\ _r}\, \mathrm{d}\boldsymbol{x} + \sum_{\in\ _t} \sum_{i \in (\ )} \int_{\Gamma_i} \boldsymbol{H}(\boldsymbol{w}_t|_{\Gamma_i}, \boldsymbol{w}_t|_{\Gamma_i}, \boldsymbol{n}_i) \cdot \boldsymbol{\varphi}_t\ \mathrm{d}, \tag{16}$$

we can define an *approximate solution* of (1) as a function $\boldsymbol{w}_h$ satisfying the conditions

$$\begin{aligned} &\text{(a)} \quad \boldsymbol{w}_t \in C^1([0, \ ]; \boldsymbol{S}_t),\\ &\text{(b)} \quad \frac{\mathrm{d}}{\mathrm{d}}(\boldsymbol{w}_t(\ ), \boldsymbol{\varphi}_t)_t + \tilde{}_t(\boldsymbol{w}_t(\ ), \boldsymbol{\varphi}_t) = 0 \quad \forall \boldsymbol{\varphi}_t \in \boldsymbol{S}_t,\ \forall \in (0, \ ),\\ &\text{(c)} \quad \boldsymbol{w}_t(0) = \Pi_t \boldsymbol{w}^0, \end{aligned} \tag{17}$$

where $\Pi_t \boldsymbol{w}^0$ is the L^2-projection of $\boldsymbol{w}^0$ from the initial condition (5) on the space $\boldsymbol{S}_h$. If we set r=0, then we obviously obtain the finite volume method.

The numerical flux $\boldsymbol{H}$ is assumed to be (locally) Lipschitz-continuous, consistent, i.e.

$$\boldsymbol{H}(\boldsymbol{w}, \boldsymbol{w}, \boldsymbol{n}) = \sum_{r=1}^{2} \boldsymbol{f}_r(\boldsymbol{w})\nu r,$$

and conservative, i.e.

$$\boldsymbol{H}(\boldsymbol{u}, \boldsymbol{w}, \boldsymbol{n}) = -\boldsymbol{H}(\boldsymbol{w}, \boldsymbol{u}, -\boldsymbol{n}).$$

3.2. Time discretization

Relation (17)(b) represents a system of ordinary differential equations, which can be solved by a suitable numerical method. Usually, *Runge–Kutta schemes* are applied. However, they are conditionally stable and

the time step is strongly limited by the CFL-stability condition. It is well known that for the discontinuous Galerkin space semidiscretization the stability condition becomes very restrictive with increasing polynomial degree r. Another possibility is to use the fully implicit *backward Euler method*, but it leads to a large system of highly nonlinear algebraic equations, whose numerical solution is rather complicated. Our aim is to obtain a higher order unconditionally stable scheme, which would require the solution of a linear system on each time level. This is carried out with the aid of a suitable partial linearization of the form $\tilde{}_t$. In what follows, we consider a partition $0 = {}_0 < {}_1 < {}_2 \cdots$ of the time interval $(0,T)$ and set $\tau = {}_{+1} - {}$. We use the symbol $\boldsymbol{w}_t$ for the approximation of $\boldsymbol{w}_t(\ )$.

In [8] we described a new DG semi-implicit technique which is suitable for an efficient solution of inviscid stationary as well as nonstationary compressible flow. This technique is based on the linearization of the form $\tilde{}_t$ carried out with the aid of the homogeneity of the fluxes $\boldsymbol{f}_s$ and the use of the Vijayasundaram numerical flux (cf. [24] or [12], Section 3.3.4). In this way we obtain the form

$$
\begin{aligned}
{}_t(\boldsymbol{w}_t, \boldsymbol{w}_t^{+1}, \boldsymbol{\varphi}_t) = & -\sum_{\in\ t} \int \sum_{r=1}^{2} \boldsymbol{A}_r(\boldsymbol{w}_t(\boldsymbol{x}))\boldsymbol{w}_t^{+1}(\boldsymbol{x}) \cdot \frac{\partial \boldsymbol{\varphi}_t(\boldsymbol{x})}{\partial\ _r}\, \mathrm{d}\boldsymbol{x} + \sum_{\in\ t} \sum_{i \in \underline{\bullet}(\ )} \int_{\Gamma_i} [\boldsymbol{P}^{+}(\langle \boldsymbol{w}_t \rangle_i, \boldsymbol{n}_i)\boldsymbol{w}_t^{+1}|_{\Gamma_i} \\
& + \boldsymbol{P}^{-}(\langle \boldsymbol{w}_t \rangle_i, \boldsymbol{n}_i)\boldsymbol{w}_t^{+1}|_{\Gamma_i}] \cdot \boldsymbol{\varphi}_t\, \mathrm{d}\underline{\bullet},
\end{aligned} \tag{18}
$$

which is linear with respect to the second argument $\boldsymbol{w}_t^{+1}$ and the third argument $\boldsymbol{\varphi}_t$. Here, $\boldsymbol{P}^{\pm} = \boldsymbol{P}^{\pm}(\boldsymbol{w}, \boldsymbol{n})$ represents the positive/negative part of the matrix $\boldsymbol{P}$ defined on the basis of its diagonalization (see, e.g. [12], Section 3.1):

$$
\boldsymbol{P} = \boldsymbol{T}\boldsymbol{D}\boldsymbol{T}^{-1}, \quad \boldsymbol{D} = \mathrm{diag}\,(\lambda_1, \ldots, \lambda_4), \tag{19}
$$

where $\lambda_1, \ldots, \lambda_4$ are the eigenvalues of $\boldsymbol{P}$. Then we set

$$
\boldsymbol{D}^{\pm} = \mathrm{diag}(\lambda_1^{\pm}, \ldots, \lambda_4^{\pm}), \quad \boldsymbol{P}^{\pm} = \boldsymbol{T}\boldsymbol{D}^{\pm}\boldsymbol{T}^{-1}, \tag{20}
$$

where $\lambda^{+} = \max\{\lambda, 0\}$ and $\lambda^{-} = \min\{\lambda, 0\}$.

On the basis of the above considerations we obtain the following semi-implicit scheme: For each $\geqslant 0$ find $\boldsymbol{w}_t^{+1}$ such that

$$
\begin{aligned}
&\text{(a)} \quad \boldsymbol{w}_t^{+1} \in \boldsymbol{S}_t, \\
&\text{(b)} \quad \left(\frac{\boldsymbol{w}_t^{+1} - \boldsymbol{w}_t}{\tau}, \boldsymbol{\varphi}_t\right)_t + {}_t(\boldsymbol{w}_t, \boldsymbol{w}_t^{+1}, \boldsymbol{\varphi}_t) = 0 \quad \forall \boldsymbol{\varphi}_t \in \boldsymbol{S}_t, \quad = 0, 1, \ldots, \\
&\text{(c)} \quad \boldsymbol{w}_t^{0} = \boldsymbol{\Pi}_t \boldsymbol{w}^{0}.
\end{aligned} \tag{21}
$$

This is a first order accurate scheme in time. In the solution of nonstationary flows, it is necessary to apply a scheme, which is sufficiently accurate in space as well as in time. One possibility is to apply the following two step second order time discretization: In (18), the second order approximation $\tilde{\boldsymbol{w}}_t^{+1}$ of $\boldsymbol{w}_t(\ _{+1})$ obtained with the aid of extrapolation,

$$
\tilde{\boldsymbol{w}}_t^{+1} = \frac{\tau\ + \tau_{-1}}{\tau_{-1}} \boldsymbol{w}_t - \frac{\tau}{\tau_{-1}} \boldsymbol{w}_t^{-1}, \tag{22}
$$

which replaces the state $\boldsymbol{w}_t$ in the form b_h, and the second order backward difference approximation of the time derivative of the solution at time t_{k+1} yield the following *two-step second-order scheme*: For each $\geqslant 1$ find $\boldsymbol{w}_t^{+1}$ such that

$$
\begin{aligned}
&\text{(a)} \quad \boldsymbol{w}_t^{+1} \in \boldsymbol{S}_t, \\
&\text{(b)} \quad \frac{2\tau\ + \tau_{-1}}{\tau\ (\tau\ + \tau_{-1})}(\boldsymbol{w}_t^{+1}, \boldsymbol{\varphi}_t)_t + {}_t(\tilde{\boldsymbol{w}}_t^{+1}, \boldsymbol{w}_t^{+1}, \boldsymbol{\varphi}_t) = \frac{\tau\ + \tau_{-1}}{\tau\ \tau_{-1}}(\boldsymbol{w}_t, \boldsymbol{\varphi}_t)_t - \frac{\tau\ (\boldsymbol{w}_t^{-1}, \boldsymbol{\varphi}_t)_t}{\tau_{-1}(\tau\ + \tau_{-1})} \\
&\qquad \forall \boldsymbol{\varphi}_t \in \boldsymbol{S}_t, \quad = 0, 1, \ldots, \\
&\text{(c)} \quad \boldsymbol{w}_t^{0} = \boldsymbol{\Pi}_t \boldsymbol{w}^{0}, \boldsymbol{w}_t^{1} \text{ obtained by the Runge–Kutta method.}
\end{aligned} \tag{23}
$$

The linear algebraic system equivalent to (21)(b) or (23)(b) is solved either by a direct solver UMFPACK [5] in case that the number of unknowns does not exceed 10^5, or by the GMRES method with a block diagonal preconditioning in case of larger systems.

In order to guarantee the stability of the scheme, we use the CFL condition

$$\tau \max_{\in \ t} \frac{1}{|\ \ |} (\max_{i \in \ell(\ )} |\Gamma_i\ | \lambda^{\max}_{\boldsymbol{P}(\boldsymbol{w}_{\ell}|_{\Gamma_i}, \boldsymbol{n}_i)}) \leqslant \mathrm{CFL}, \tag{24}$$

where $|\ \ |$ denotes the area of K_i, $|\Gamma_i\ |$ the length of the edge Γ_{ij}, CFL a given constant and $\lambda^{\max}_{\boldsymbol{P}(\boldsymbol{w}_{\ell}|_{\Gamma_i}, \boldsymbol{n}_i)}$ is the maximal eigenvalue of the matrix $\boldsymbol{P}(\boldsymbol{w}_{\ell}|_{\Gamma_i}, \boldsymbol{n}_i)$ defined by (7), where the maximum is taken over Γ_{ij}. Numerical experiments show that the CFL number can be practically unlimited.

4. Boundary conditions

If $\Gamma_i \subset \partial\Omega_{\ell}$, i.e. $i \in \gamma(\ )$, it is necessary to specify the boundary state $\boldsymbol{w}|_{\Gamma_i}$ appearing in the numerical flux $\boldsymbol{H}$ in the definition of the inviscid form b_h. The appropriate treatment of boundary conditions plays a crucial role in the solution of low Mach number flows.

If Γ_{ij} is a part of a fixed impermeable wall, then $\boldsymbol{v} \cdot \boldsymbol{n} = 0$ and we use the approximation

$$\int_{\Gamma_i} \boldsymbol{H}(\boldsymbol{w}_{\ell}^{+1}|_{\Gamma_i}, \boldsymbol{w}_{\ell}^{+1}|_{\Gamma_i}, \boldsymbol{n}_i) \cdot \boldsymbol{\varphi}_{\ell}\ \mathrm{d}\ell \approx \int_{\Gamma_i} \boldsymbol{F}\ \ (\boldsymbol{w}_{\ell}, \boldsymbol{w}_{\ell}^{+1}, \boldsymbol{n}_i) \cdot \boldsymbol{\varphi}_{\ell}\ \mathrm{d}\ell, \tag{25}$$

where $\boldsymbol{F}_W$ is obtained from (6), where we set $\boldsymbol{v} \cdot \boldsymbol{n} = 0$, apply the linearization with the aid of the Taylor expansion and use (10). In this way we obtain

$$\boldsymbol{F}\ \ (\boldsymbol{w}_{\ell}, \boldsymbol{w}_{\ell}^{+1}, \boldsymbol{n}) = \boldsymbol{P}(\boldsymbol{w}_{\ell}, \boldsymbol{n}) \boldsymbol{w}_{\ell}^{+1}. \tag{26}$$

Under the condition $\boldsymbol{v} \cdot \boldsymbol{n} = 0$ we have

$$\boldsymbol{P}(\boldsymbol{w}, \boldsymbol{n}) = (\gamma - 1) \begin{pmatrix} 0 & 0 & 0 & 0 \\ (\cdot\ \frac{2}{1} + \cdot\ \frac{2}{2})\kappa 1/2 & -\cdot\ _{1}\kappa 1 & -\cdot\ _{2}\kappa 1 & \kappa 1 \\ (\cdot\ \frac{2}{1} + \cdot\ \frac{2}{2})\kappa 2/2 & -\cdot\ _{1}\kappa 2 & -\cdot\ _{2}\kappa 2 & \kappa 2 \\ 0 & 0 & 0 & 0 \end{pmatrix}. \tag{27}$$

On the inlet and outlet it is necessary to use nonreflecting boundary conditions transparent for acoustic effects coming from inside of Ω. Therefore, *characteristics based* boundary conditions are used.

Using the rotational invariance, we transform the Euler equations to the coordinates $\tilde{}_1$, parallel with the normal direction $\boldsymbol{n}_i$ to the boundary, and $\tilde{}_2$, tangential to the boundary, neglect the derivative with respect to $\tilde{}_2$ and linearize the system around the state $\boldsymbol{q}_i = \boldsymbol{Q}(\boldsymbol{n}_i)\boldsymbol{w}|_{\Gamma_i}$, where

$$\boldsymbol{Q}(\boldsymbol{n}_i) = \begin{pmatrix} 1, & 0, & 0, & 0 \\ 0, & (\kappa i)_1, & (\kappa i)_2, & 0 \\ 0, & -(\kappa i)_2, & (\kappa i)_1, & 0 \\ 0, & 0, & 0, & 1 \end{pmatrix} \tag{28}$$

is the rotational matrix. Then we obtain the linear system

$$\frac{\partial \boldsymbol{q}}{\partial} + \boldsymbol{A}_1(\boldsymbol{q}_i) \frac{\partial \boldsymbol{q}}{\partial \tilde{}_1} = 0, \tag{29}$$

for the transformed vector-valued function $\boldsymbol{q} = \boldsymbol{Q}(\boldsymbol{n}_i)\boldsymbol{w}$, considered in the set $(-\infty, 0) \times (0, \infty)$ and equipped with the initial and boundary conditions

$$\begin{aligned} &\boldsymbol{q}(\tilde{}_1, 0) = \boldsymbol{q}_i\ , \quad \tilde{}_1 < 0, \\ &\boldsymbol{q}(0,\ ) = \boldsymbol{q}_{\ell}\ , \quad > 0. \end{aligned} \tag{30}$$

The goal is to choose $\boldsymbol{q}_{ji}$ in such a way that this initial-boundary value problem is well posed, i.e. has a unique solution. The method of characteristics leads to the following process:

Let us put $\boldsymbol{q}_i^* = \boldsymbol{Q}(\boldsymbol{n}_i)\boldsymbol{w}_i^*$, where $\boldsymbol{w}_i^*$ is a given boundary state at the inlet or outlet. We calculate the eigenvectors $\boldsymbol{r}_s$ corresponding to the eigenvalues λ_r, $r = 1, \ldots, 4$, of the matrix $\boldsymbol{A}_1(\boldsymbol{q}_i)$, arrange them as columns in the matrix $\boldsymbol{T}$ and calculate $\boldsymbol{T}^{-1}$ (explicit formulae can be found in [12], Section 3.1). Now we set

$$\boldsymbol{\alpha} = \boldsymbol{T}^{-1}\boldsymbol{q}_i\,, \quad \boldsymbol{\beta} = \boldsymbol{T}^{-1}\boldsymbol{q}_i^* \tag{31}$$

and define the state $\boldsymbol{q}_{ji}$ by the relations

$$\boldsymbol{q}_{ji} := \sum_{r=1}^{4} \gamma_r \boldsymbol{r}_r, \quad \gamma_r = \begin{cases} \alpha_r, & \lambda_r \geqslant 0, \\ \beta_r, & \lambda_r < 0. \end{cases} \tag{32}$$

Finally, the sought boundary state $\boldsymbol{w}|_{\Gamma_i}$ is defined as

$$\boldsymbol{w}|_{\Gamma_i} = \boldsymbol{w}_{ji} = \boldsymbol{Q}^{-1}(\boldsymbol{n}_i)\boldsymbol{q}_{ji}\,. \tag{33}$$

5. Shock capturing

For high speed flows with shock waves and contact discontinuities it is necessary to avoid the Gibbs phenomenon manifested by spurious overshoots and undershoots in computed quantities near discontinuities and steep gradients. These phenomena do not occur in low Mach number regimes, however in the transonic case they cause instabilities in the semi-implicit solution.

One possibility for avoiding the Gibbs phenomenon is the use of the limiting of order of accuracy of the method in the vicinity of discontinuities. The limiting technique is motivated by the paper [16], on the basis of which the left-hand side of (21)(b) and (23)(b) is augmented by an artificial viscosity form. However, since this form is nonzero also in regions, where the exact solution is regular, a small nonphysical entropy production can appear in these regions. Therefore, we combine this technique with the approach proposed in [10]. It is based on the discontinuity indicator $g^k(i)$ defined by

$$b\,(\,) = \int_{\partial} [\rho_t]^2 \,\mathrm{d}\underline{\bullet}/(\underline{\bullet} \quad | \quad |^{3/4}), \qquad \in \quad t\,, \tag{34}$$

in the 2D case. (By $[\rho_t]$ we denote the jump of the density on ∂K_i at time t_k.) The indicator $g^k(i)$ was constructed in such a way that it takes an anisotropy of the computational mesh into account. It was shown in [10] that the indicator $g^k(i)$ identifies discontinuities safely on unstructured and anisotropic meshes. Now we introduce the discrete discontinuity indicator

$$(\,) = 0 \quad \text{if } b\,(\,) < 1, \qquad (\,) = 1, \quad \text{if } b\,(\,) \geqslant 1, \qquad \in \quad t\,, \tag{35}$$

and add the artificial viscosity form

$$\beta_t(\boldsymbol{w}_t, \boldsymbol{w}_t^{+1}, \boldsymbol{\varphi}) = v_1 \sum_{\in} \underline{\bullet} \qquad (\,) \int \nabla \boldsymbol{w}_t^{+1} \cdot \nabla \boldsymbol{\varphi}\,\mathrm{d}\boldsymbol{x} \tag{36}$$

with $v_1 = \mathrm{O}(1)$ to the left-hand side of (21)(b) and (23)(b). Because the artificial viscosity form is rather local, we propose to augment the left-hand side of (21)(b) and (23)(b) by adding the form

$$\nu_t(\boldsymbol{w}_t, \boldsymbol{w}_t^{+1}, \boldsymbol{\varphi}) = v_2 \sum_{\in} \sum_{i \in r(\,)} \frac{1}{2}(\quad (\,) + \quad (\,)) \int_{\Gamma_i} [\boldsymbol{w}_t^{+1}] \cdot [\boldsymbol{\varphi}]\,\mathrm{d}\underline{\bullet}, \tag{37}$$

where $v_2 = \mathrm{O}(1)$, which allows to strengthen the influence of neighbouring elements and improves the behaviour of the method in the case, when strongly unstructured and/or anisotropic meshes are used.

Thus, the resulting scheme obtained by limiting of (21)(b) reads:

$$\begin{aligned}
&\text{(a)} \quad \boldsymbol{w}_t^{+1} \in \boldsymbol{S}_t,\\
&\text{(b)} \quad \left(\frac{\boldsymbol{w}_t^{+1}-\boldsymbol{w}_t}{\tau}, \boldsymbol{\varphi}_t\right)_t + \quad_t(\boldsymbol{w}_t, \boldsymbol{w}_t^{+1}, \boldsymbol{\varphi}_t) + \beta_t(\boldsymbol{w}_t, \boldsymbol{w}_t^{+1}, \boldsymbol{\varphi}_t) + \nu_t(\boldsymbol{w}_t, \boldsymbol{w}_t^{+1}, \boldsymbol{\varphi}_t) = 0\\
&\qquad \forall \boldsymbol{\varphi}_t \in \boldsymbol{S}_t, \quad = 0, 1, \ldots,\\
&\text{(c)} \quad \boldsymbol{w}_t^0 = \Pi_t \boldsymbol{w}^0.
\end{aligned} \tag{38}$$

(Similarly, we obtain a stabilized version of scheme (23).)

This method successfully overcomes problems with the Gibbs phenomenon in the context of the semi-implicit scheme. It is important to note that $G^k(i)$ vanishes in regions, where the solution is regular. Therefore, the scheme does not produce any nonphysical entropy in these regions (see Fig. 12).

Remark 1. In order to obtain an accurate, physically admissible solution, it is necessary to use isoparametric elements near curved boundaries (see [1] or [7]). In our computations we proceed in such a way that a reference triangle is transformed by a bilinear mapping onto the approximation of a curved triangle adjacent to the boundary $\partial\Omega$.

6. Numerical examples

In this section, we present the solution of some test problems in order to demonstrate the accuracy and robustness of the proposed method. The computational grids were constructed with the aid of the anisotropic mesh adaptation technique [6]. In all examples quadratic elements ($r = 2$) were applied. Steady state solutions were obtained via time stabilization for "$\to \infty$". This means that scheme (38) was used as an iterative process for "$\to \infty$". This process was stopped, when the approximation of the time derivative satisfied the condition

$$\left\| \frac{\boldsymbol{w}_t^{+1}-\boldsymbol{w}_t}{\tau} \right\|_{\infty(\Omega)} < 10^{-8}. \tag{39}$$

6.1. Low Mach number flow

6.1.1. Irrotational flow past a Joukowski airfoil

First we consider flow past a negatively oriented Joukowski profile given by parameters $\Delta = 0.07$, $= 0.5$, $= 0.05$ (under the notation from [11], Section 2.2.68) with zero angle of attack. The far field quantities are constant, which implies that the flow is irrotational and homoentropic. Using the complex function method from [11], we can obtain the exact solution of incompressible inviscid irrotational flow satisfying the Kutta–Joukowski trailing condition, provided the velocity circulation around the profile, related to the magnitude of the far field velocity, $\gamma_{\text{ref}} = 0.7158$. We assume that the far field Mach number of compressible flow $_\infty = 0.0001$. The computational domain is of the form of a square with side of the length equal to 10 chords of the profile. The mesh (in the whole computational domain) was formed by 5418 triangular elements and refined towards the profile. Fig. 1 shows a detail near the profile of the velocity isolines for the exact solution of incompressible flow and for the approximate solution of compressible flow. In Fig. 2, pressure isolines of incompressible and compressible flow are plotted. Fig. 3 shows streamlines of the computed compressible flow. We see that the flow past the trailing edge is smooth. Further, in Figs. 4 and 5, the velocity distribution and pressure coefficient distribution, respectively, past the profile is plotted in the direction from the leading edge to the trailing edge (∘ ∘ ∘ – exact solution of incompressible flow, — – approximate solution of compressible flow). The pressure coefficient was defined as $10^7 \cdot (\quad - \quad_\infty)$, where p_∞ denotes the far field pressure.

The maximum density variation is 1.04×10^{-8}. The computed velocity circulation related to the magnitude of the far field velocity is $\gamma_{\text{refcomp}} = 0.7205$, which gives the relative error 0.66% with respect to the theoretical value γ_{ref} obtained for incompressible flow.

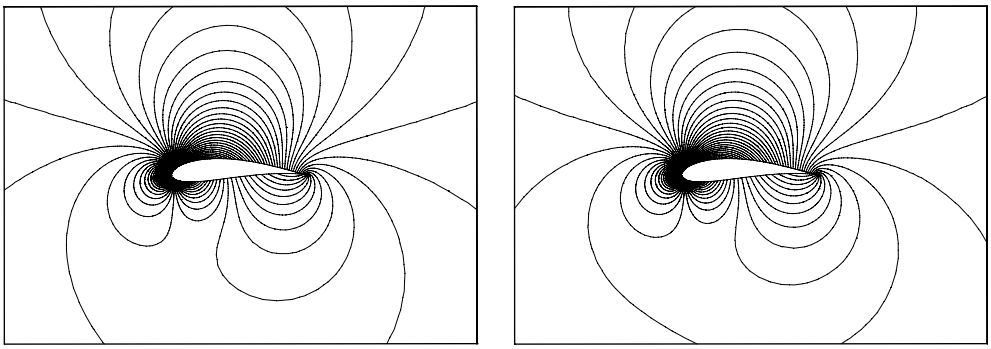

Fig. 1. Velocity isolines for the exact solution of incompressible flow (left) and approximate solution of compressible flow (right).

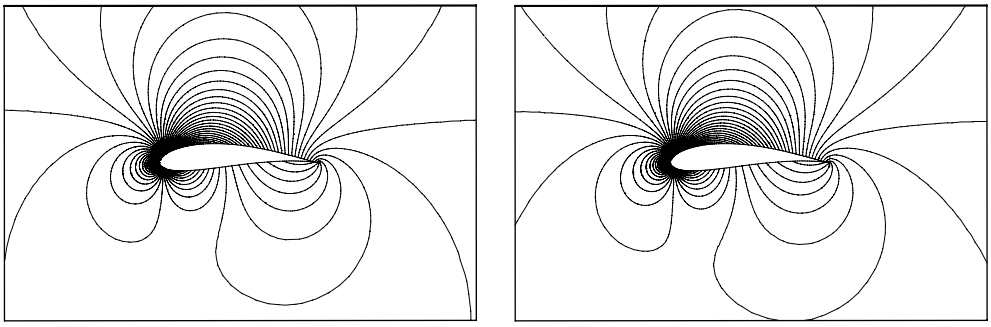

Fig. 2. Pressure isolines for the exact solution of incompressible flow (left) and approximate solution of compressible flow (right).

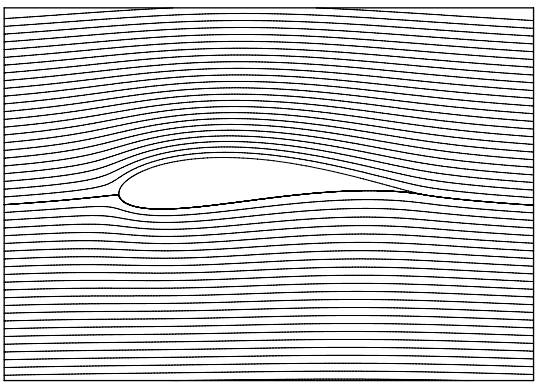

Fig. 3. Compressible flow past a Joukowski profile, approximate solution, streamlines.

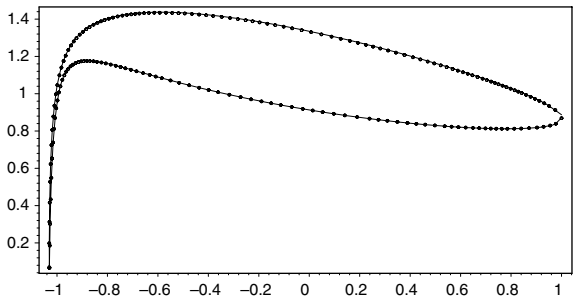

Fig. 4. Flow past a Joukowski profile, velocity distribution along the profile: ○ ○ ○ – exact solution of incompressible flow, — – approximate solution of compressible flow.

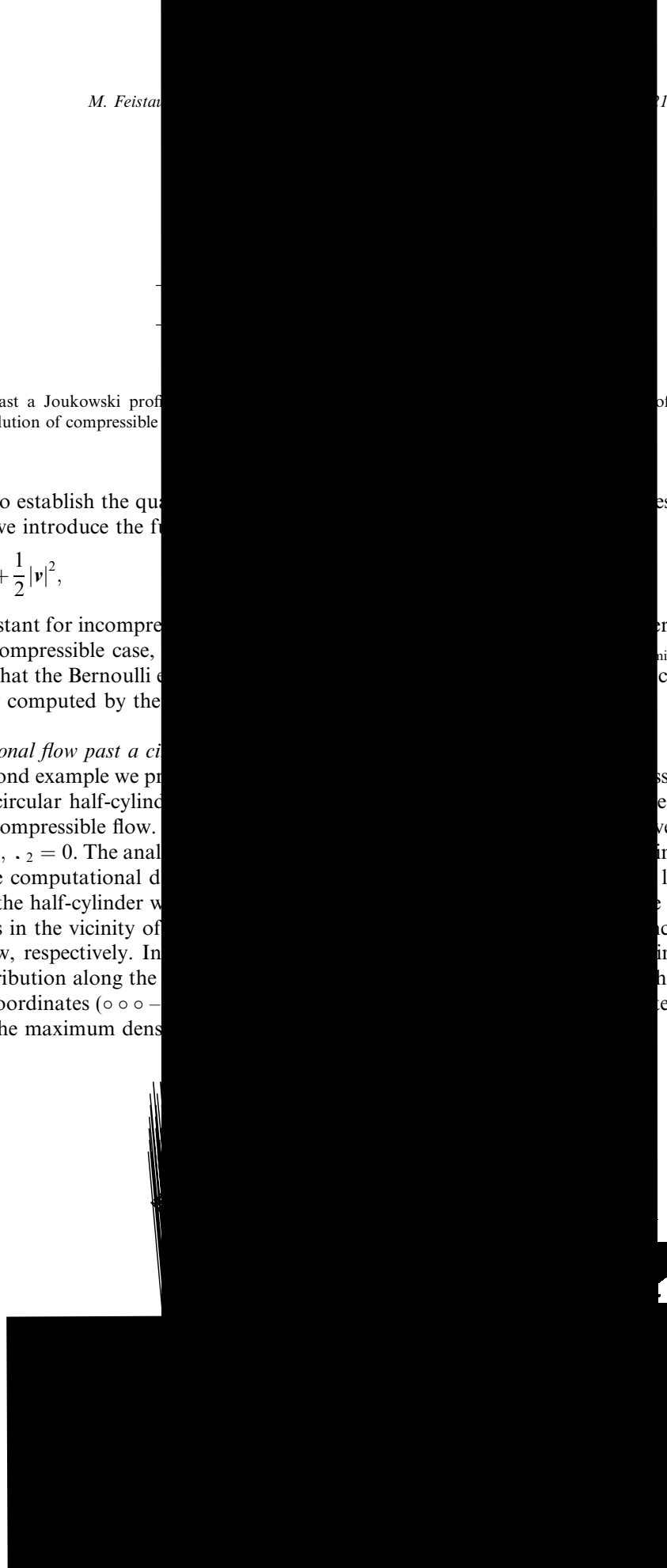

Fig. 5. Flow past a Joukowski prof of incompressible flow, — – approximate solution of compressible

In order to establish the qu essible flow in a quanti-
tative way, we introduce the f

$$B = \frac{}{\rho} + \frac{1}{2}|\boldsymbol{v}|^2, \tag{40}$$

which is constant for incompre rnoulli equation. In the
considered compressible case, $_{\min})/B_{\max} = 3.84 \times 10^{-6}$.
This means that the Bernoulli e compressible low Mach
number flow computed by the

6.1.2. Rotational flow past a ci

In the second example we pr ssible inviscid rotational
flow past a circular half-cylinc e, with an approximate
solution of compressible flow. velocity has the compo-
nents $_1 = \ _2$, $_2 = 0$. The anal interesting for its corner
vortices. The computational d length 10 and width 5,
from which the half-cylinder w e present here computa-
tional results in the vicinity of compressible and com-
pressible flow, respectively. In ines. Fig. 10 shows the
velocity distribution along the here ϑ is the angle from
cylindrical coordinates ($\circ\circ\circ$ – e solution of compress-
ible flow). The maximum dens

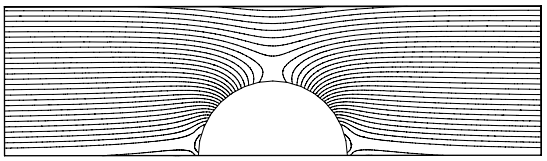

Fig. 8. Rotational incompressible flow past a half-cylinder, exact solution, velocity isolines.

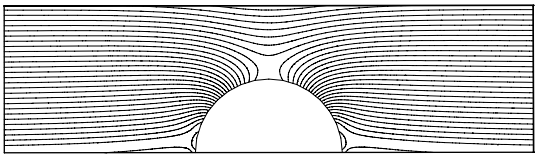

Fig. 9. Rotational compressible flow past a half-cylinder, approximate solution, velocity isolines.

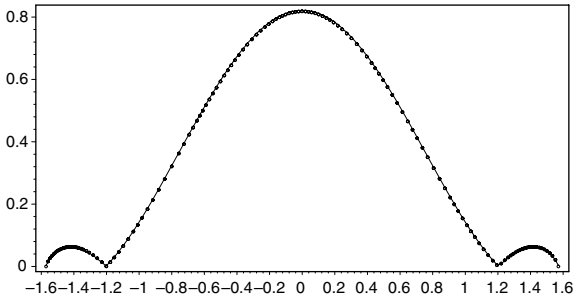

Fig. 10. Rotational flow past a half-cylinder, velocity distribution on the half-cylinder: ∘ ∘ ∘ – exact solution of incompressible flow, — – approximate solution of compressible flow.

6.1.3. Accuracy of the method

An interesting question is the order of accuracy of the semi-implicit DG method. Theoretical analysis of a one-step semi-implicit DG scheme applied to a scalar nonstationary nonlinear convection–diffusion problem is contained in [9].

We tested numerically the accuracy of the piecewise quadratic DG approximations of the stationary inviscid flow past a circular cylinder with the far field velocity parallel to the axis x_1 and the Mach number $_\infty = 10^{-4}$. The problem was solved in a computational domain of the form of a square with sides of the length equal to 20 diameters of the cylinder. Table 1 presents the behaviour of the error and experimental order of convergence (EOC) of the approximate solution $\boldsymbol{w}_h$ of compressible flow to the exact incompressible solution, measured in $^\infty(\Omega_t)$-norm. We see that the experimental order of convergence is close to 2.5, which is comparable to theoretical error estimates obtained (for $^2(\Omega)$-norm) in [13].

Table 1
Error in L^∞-norm and corresponding experimental order of convergence for the approximation of incompressible flow by low Mach number compressible flow with respect to $\ \to 0$

# $_t$	$\|\text{error}\|_{\infty(\Omega_t)}$	EOC
1251	5.05E−01	–
1941	4.23E−01	0.406
5031	2.77E−02	2.86
8719	6.68E−03	2.59

6.2. Transonic flow

The possibility to apply the proposed method to high speed f
terms from Section 5 is tested on the flow through the GAMM ch
Mach number equal to 0.67. In this case a conspicuous shock wa
number isolines and entropy isolines computed by scheme (38). O
production on the shock wave only, which is correct from the p
distribution on the lower wall is plotted. We see that the shock
resolved Zierep singularity (small local maximum). The maximu

In this case the computational mesh was formed by 7753 eleme
shock wave.) The stabilization parameters in scheme (38) were
show that these coefficients give good results also for other prob
cess, e.g. for the solution of transonic and hypersonic flow past

It follows from the examples presented in Section 6.1 that the
tion of compressible flow with low Mach numbers. The comp
approximate very well the corresponding incompressible flows.

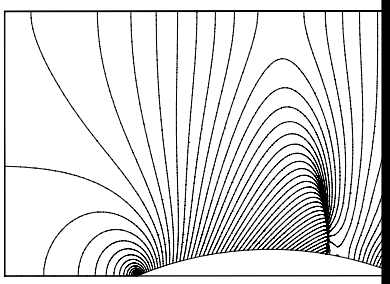

Fig. 11. Transonic flow through the GAMM chan

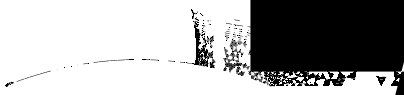

Fig. 12. Transonic flow through the GAMM channel, entropy

Fig. 13. Transonic flow through the GAMM channel, density

in comparison with the transonic example. This means that the computed low Mach number flow behaves as incompressible flow. Section 6.2 demonstrates that the method is also suitable for the numerical solution of high speed transonic flow.

In the computational process, the CFL number from the stability condition (24) can be chosen very large. Namely, during the computational process, the CFL number was successively increased from 30 up to 3×10^3 or 3×10^6 in the case of transonic flow from Section 6.2 or in the case of low Mach number flows from Section 6.1, respectively. Thus, the scheme is practically *unconditionally stable*.

7. Conclusion

We have presented an efficient higher-order numerical scheme for the solution of the compressible Euler equations. It is based on several important ingredients:

- the application of the discontinuous Galerkin method for the space discretization,
- special treatment of boundary conditions,
- semi-implicit time discretization,
- suitable limiting of the order of accuracy in the vicinity of discontinuities,
- the use of superparametric elements near curved parts of the boundary.

The presented method behaves as unconditionally stable and appears to be robust with respect to the magnitude of the Mach number. It allows the numerical solution of high speed transonic flow as well as low Mach number flow, using the Euler equations in the conservation form with conservative variables.

The method was tested on several examples proving its accuracy and robustness with respect to the Mach number. The comparison of the developed semi-implicit method with explicit Runge–Kutta schemes shows that the Runge–Kutta schemes fail, when they are applied to the solution of low Mach number flows, in contrast to the semi-implicit method. It follows from numerical experiments carried out in [8] that even for higher Mach number flows the semi-implicit method appears more efficient than the Runge–Kutta methods.

Future work will be concentrated on the extension of the method to the solution of compressible viscous flow, combining the DGFEM with anisotropic mesh adaptation. Another important issue is the theoretical justification of the developed technique using a multiscale analysis or finding limitations of this method with respect to results obtained in [15]. This represents a difficult and completely open problem.

Acknowledgments

We wish to express our sincere gratitude to Professor Phil Roe for providing Ref. [14] on the exact solution of a rotational incompressible flow problem and the recommendation to test our method on this interesting nonstandard example. This work is a part of the research project No. MSM 0021620839 of the Ministry of Education of the Czech Republic. The research of M. Feistauer was partly supported by the Grant No. 201/05/0005 of the Czech Grant Agency. The research of V. Kučera was partly supported by the Grant No. 6/2005/R of the Grant Agency of the Charles University and by the Necas Center – Project LC 06052 financed by the Ministry of Education of the Czech Republic. The authors acknowledge the support of these institutions.

References

[1] F. Bassi, S. Rebay, High-order accurate discontinuous finite element solution of the 2D Euler equations, J. Comput. Phys. 138 (1997) 251–285.

[2] C.E. Baumann, J.T. Oden, A discontinuous *hp* finite element method for the Euler and Navier–Stokes equations, Int. J. Numer. Methods Fluids 31 (1999) 79–95.

[3] B. Cockburn, G.E. Karniadakis, C.-W. Shu (Eds.), Discontinuous Galerkin Methods, Lecture Notes in Computational Science and Engineering, vol. 11, Springer, Berlin, 2000.

[4] M. Darwish, F. Moukalled, B. Sekar, A robust multi-grid pressure-based algorithm for multi-fluid flow at all speeds, Int. J. Numer. Methods Fluids 41 (2003) 1221–1251.

[5] T.A. Davis, I.S. Duff, A combined unifrontal/multifrontal method for unsymmetric sparse matrices, ACM Trans. Math. Software 25 (1999) 1–19.
[6] V. Dolejší, Anisotropic mesh adaptation for finite volume and finite element methods on triangular meshes, Comput. Vis. Sci. 1 (3) (1998) 165–178.
[7] V. Dolejší, M. Feistauer, On the discontinuous Galerkin method for the numerical solution of compressible high-speed flow, in: F. Brezzi, A. Buffa, S. Corsaro, A. Murli (Eds.), Numerical Mathematics and Advanced Applications, ENUMATH 2001, Springer-Verlag Italia, Milano, 2003, pp. 65–84.
[8] V. Dolejší, M. Feistauer, A semi-implicit discontinuous Galerkin finite element method for the numerical solution of inviscid compressible flow, J. Comput. Phys. 198 (2004) 727–746.
[9] V. Dolejší, M. Feistauer, J. Hozman, Analysis of semi-implicit DGFEM for nonlinear convection–diffusion problems on nonconforming meshes. Comput. Methods Appl. Mech. Eng. (in press), doi:10.1016/j.cma.2006.09.025.
[10] V. Dolejší, M. Feistauer, C. Schwab, On some aspects of the discontinuous Galerkin finite element method for conservation laws, Math. Comput. Simul. 61 (2003) 333–346.
[11] M. Feistauer, Mathematical Methods in Fluid Dynamics, Longman Scientific & Technical, Harlow, 1993.
[12] M. Feistauer, J. Felcman, I. Straškraba, Mathematical and Computational Methods for Compressible Flow, Clarendon Press, Oxford, 2003.
[13] M. Feistauer, K. Švadlenka, Discontinuous Galerkin method of lines for solving nonstationary singularly perturbed linear problems, J. Numer. Math. 2 (2004) 97–117.
[14] L. Fraenkel, On corner eddies in plane inviscid shear flow, J. Fluid Mech. 11 (1961) 400–406.
[15] G. Hauke, T.J.R. Hughes, A comparative study of different sets of variables for solving compressible and incompressible flows, Comput. Methods Appl. Mech. Eng. 153 (1998) 1–44.
[16] J. Jaffre, C. Johnson, A. Szepessy, Convergence of the discontinuous Galerkin finite elements method for hyperbolic conservation laws, Math. Models Methods Appl. Sci. 5 (1995) 367–386.
[17] R. Klein, Semi-implicit extension of a Godunov-type scheme based on low Mach number asymptotics 1: one-dimensional flow, J. Comput. Phys. 121 (1995) 213–237.
[18] A. Meister, Viscous flow fields at all speeds: analysis and numerical simulation, J. Appl. Math. Phys. 54 (2003) 1010–1049.
[19] A. Meister, J. Struckmeier, Hyperbolic Partial Differential Equations, Theory, Numerics and Applications, Vieweg, Braunschweig, 2002.
[20] J.H. Park, C.-D. Munz, Multiple pressure variables methods for fluid flow at all Mach numbers, Int. J. Numer. Methods Fluids 49 (2005) 905–931.
[21] S. Roller, C.-D. Munz, K.J. Geratz, R. Klein, The multiple pressure variables method for weakly compressible fluids, Z. Angew. Math. Mech. 77 (1997) 481–484.
[22] D.R. van der Heul, C. Vuik, P. Wesseling, A conservative pressure-correction method for flow at all speeds, Comput. Fluids 32 (2003) 1113–1132.
[23] J.J.W. van der Vegt, H. van der Ven, Space–time discontinuous Galerkin finite element method with dynamic grid motion for inviscid compressible flow, J. Comput. Phys. 182 (2002) 546–585.
[24] G. Vijayasundaram, Transonic flow simulation using upstream centered scheme of Godunov type in finite elements, J. Comput. Phys. 63 (1986) 416–433.
[25] I. Wenneker, A. Segal, P. Wesseling, A Mach-uniform unstructured staggered grid method, Int. J. Numer. Methods Fluids 40 (2002) 1209–1235.
[26] P. Wesseling, Principles of Computational Fluid Dynamics, Springer, Berlin, 2001.
[27] P. Wesseling, D.R. van der Heul, Uniformly effective numerical methods for hyperbolic systems, Computing 66 (2001) 249–267.